β-Bi_2O_3 under compression: Optical and elastic properties and electron density topology analysis

A. L. J. Pereira,[1,2] O. Gomis,[3,*] J. A. Sans,[1] J. Contreras-García,[4] F. J. Manjón,[1] P. Rodríguez-Hernández,[5] A. Muñoz,[5] and A. Beltrán[6]

[1]*Instituto de Diseño para la Fabricación y Producción Automatizada, MALTA Consolider Team, Universitat Politècnica de València, València, Spain*

[2]*Grupo de Pesquisa em Materiais Fotônicos e Energia Renovável - MaFER, Faculdade de Ciências Exatas e Tecnologia, Universidade Federal da Grande Dourados, Dourados, Brazil*

[3]*Centro de Tecnologías Físicas: Acústica, Materiales y Astrofísica, MALTA Consolider Team, Universitat Politècnica de València, València, Spain*

[4]*Laboratoire de Chimie Théorique, Université Pierre et Marie Curie, F-75005 Paris, France*

[5]*Departamento de Física, Instituto de Materiales y Nanotecnología, MALTA Consolider Team, Universidad de La Laguna, La Laguna, Tenerife, Spain*

[6]*Departament de Química Física i Analítica, MALTA Consolider Team, Universitat Jaume I, Castello de la Plana, Spain*

(Received 22 January 2016; revised manuscript received 18 April 2016; published 30 June 2016)

We report a joint experimental and theoretical study of the optical properties of tetragonal bismuth oxide (β-Bi_2O_3) at high pressure by means of optical absorption measurements combined with *ab initio* electronic band structure calculations. Our results are consistent with previous results that show the presence of a second-order isostructural phase transition in Bi_2O_3 (from β to β') around 2 GPa and a phase transition above 15 GPa combined with a pressure-induced amorphization above 17–20 GPa. In order to further understand the pressure-induced phase transitions and amorphization occurring in β-Bi_2O_3, we theoretically studied the mechanical and dynamical stability of the tetragonal structures of β- and β'-Bi_2O_3 at high pressure through calculations of their elastic constants, elastic stiffness coefficients, and phonon dispersion curves. The pressure dependence of the elastic stiffness coefficients and phonon dispersion curves confirms that the isostructural phase transition near 2 GPa is of ferroelastic nature. Furthermore, a topological study of the electron density shows that the ferroelastic transition is not caused by a change in number of critical points (cusp catastrophe), but by the equalization of the electron densities of both independent O atoms in the unit cell due to a local rise in symmetry. Finally, from theoretical simulations, β'-Bi_2O_3 is found to be mechanically and dynamically stable at least up to 26.7 GPa under hydrostatic conditions; thus, the pressure-induced amorphization reported above 17–20 GPa in powder β'-Bi_2O_3 using methanol-ethanol-water as pressure-transmitting medium could be related to the frustration of a reconstructive phase transition at room temperature and the presence of mechanical or dynamical instabilities under nonhydrostatic conditions.

DOI: 10.1103/PhysRevB.93.224111

I. INTRODUCTION

A significant increase in the number of published works related to group-15 sesquioxides has occurred in the last two decades. In particular, works related to bismuth oxide (Bi_2O_3) have doubled in the last decade, thus reflecting the scientific, technological, and industrial importance of this compound. Its peculiar properties, including a large energy gap, a high refractive index and dielectric permittivity, and good photoconductivity [1–6], have made Bi_2O_3 suitable for a large range of applications, such as optical coatings, photovoltaic cells, microwave integrated circuits, fuel cells, oxygen sensors, oxygen pumps, and catalytic activity [3,7–13].

The compounds of the group-15 sesquioxide family (As_2O_3, Sb_2O_3, and Bi_2O_3) crystallize in a number of polymorphs. Their structures can be understood in many cases as derived from a defective fluorite structure by means of symmetry-breaking atomic local distortions, with the activity of the cation lone electron pair (LEP) of group-15 elements being one of the main factors determining the stabilities of the different polymorphs [14,15]. In fact, the presence of cation-centered LEPs, such as those in Pb^{2+}, As^{3+}, Sb^{3+}, and Bi^{3+}, are tremendously important for applications that require off-centered polyhedra and their associated dipoles in ferroelectric, piezoelectric, and multiferroic materials, actuators, nonlinear materials, ionic conductors, and high-refractive index materials, e.g., $BiFeO_3$ [16].

Notably, the most recent studies of Bi_2O_3 at room conditions have been mainly devoted to the photocatalytic properties of two polymorphs: α-Bi_2O_3 (bismite) and β-Bi_2O_3 (sphaerobismoite) [17–23]. In particular, it has been found that the metastable β phase exhibits better properties, in particular, better photocatalytic activity, than the more stable α phase [17–21] because of the unique tunnel structure of β-Bi_2O_3 caused by the special orientation of Bi LEPs. The tunnel structure of β-Bi_2O_3 is ideal for the transfer of the photogenerated electrons and holes, preventing their excessive recombination and enabling more free carriers to participate in the photodecomposition process [24]. In this respect, it is worth mentioning that the recent observation of the β-Bi_2O_3 phase in compressed α-Sb_2O_3 [25] could lead to the stabilization of this phase in Sb_2O_3, thus leading to novel catalytic properties of this Sb-related compound because Sb has a more active LEP than Bi in β-Bi_2O_3. Therefore, an understanding of the properties of β-Bi_2O_3 is of primary importance for its own technological applications and those of related compounds.

*Corresponding author: osgohi@fis.upv.es

In a recent work, we performed an experimental and theoretical study of the structural and vibrational properties of synthetic β-Bi_2O_3 at room temperature by means of x-ray diffraction (XRD) and Raman scattering (RS) measurements at different pressures [26]. It was observed that this compound undergoes a second-order isostructural phase transition (IPT) from the β phase to the β' phase around 2 GPa. Our theoretical lattice dynamics calculations suggested that the IPT is of displacive second-order type, and it is driven by one optical nonpolar soft mode, whose frequency goes to zero near 2 GPa and which couples to other eight optical modes. All eigenvectors of the nine soft coupled modes displace atoms towards more symmetric positions than those present in the β phase [26]. Moreover, our XRD experiments suggested the onset of a pressure-induced amorphization (PIA) of the β' structure above 17–20 GPa. This result contrasted with our RS measurements above 15 GPa, which presented some weak peaks probably related to an unknown phase observed even at 27 GPa [26].

Continuing with our study of the properties of group-15 sesquioxides, we report in this work a detailed experimental and theoretical study of the optical properties of β-Bi_2O_3 up to 26.7 GPa by means of optical absorption measurements combined with *ab initio* total-energy calculations. We will show that there is a considerable change of the indirect bandgap behavior in the β and β' phases followed by a decrease of the indirect bandgap above 15 GPa. These results are consistent with the IPT and also with the phase transition above 15 GPa and PIA above 17–20 GPa previously reported [26]. Furthermore, we performed lattice dynamics calculations at high pressures and evaluated the pressure dependence of the elastic stiffness coefficients and phonon dispersion curves. These calculations allow us to discuss the mechanical and dynamical stability of β-Bi_2O_3 and β'-Bi_2O_3 at high pressures. Our calculations show that the β-to-β' IPT in Bi_2O_3 is indeed a ferroelastic phase transition, which, according to the analysis of the topology of the electron density, occurs due to the equalization of the electron densities of both independent O atoms in the unit cell. In addition, our theoretical calculations show that β'-Bi_2O_3 is mechanically and dynamically stable up to 26.7 GPa under hydrostatic conditions. Therefore, we suggest that PIA could occur above 17–20 GPa in powders of β'-Bi_2O_3 using methanol-ethanol-water as pressure-transmitting medium due to kinetic constraints of the phase transition occurring above 15 GPa at room temperature and the presence of mechanical or dynamical instabilities of the β' structure under certain shear deformations that occur under nonhydrostatic conditions.

II. EXPERIMENTAL DETAILS

Synthetic β-Bi_2O_3 powder samples used in the present experiments were purchased from Sigma-Aldrich, Inc., with grade purity higher than 99.9%. High-pressure optical absorption experiments at room temperature up to 26.7 GPa were performed by the sample-in–sample-out method using a micro-optical system [27] in combination with a tungsten lamp and an Ocean Optics spectrometer. Powder samples were loaded in a membrane-type diamond anvil cell (DAC) and slightly compressed between the two diamonds in order to form a transparent thin sample (around 5 μm thick) with parallel faces composed of compacted powders stuck onto one of the diamond windows. This sample was then reduced to a lateral size of $100 \times 100\,\mu m^2$ and loaded inside a DAC with a 16:3:1 methanol-ethanol-water mixture as pressure-transmitting medium and ruby grains for pressure calibration with the ruby fluorescence method [28]. For optical measurements, stray light was measured in the high-absorption region of the sample for every spectrum and subtracted from the transmission spectrum. Afterwards, the experimental transmittance spectrum was scaled to the theoretical transmittance value in the spectral range where the sample is completely transparent. Finally, the absorption coefficient α was obtained from the scaled transmittance by taking into account the sample thickness and reflectivity [29].

III. THEORETICAL DETAILS

Ab initio total-energy calculations were performed within the framework of density functional theory (DFT) [30]. The VASP package [31] was used to carry out calculations with the pseudopotential method and the projector-augmented wave (PAW) [32] scheme, which replace core electrons and make smoothed pseudovalence wave functions while taking into account the full nodal character of the all-electron charge density in the core region. For bismuth, 15 valence electrons ($5d^{10}6s^26p^3$) were used, whereas for oxygen, 6 valence electrons ($2s^22p^4$) were used. The set of plane waves was extended up to a kinetic energy cutoff of 520 eV to achieve highly converged results. The exchange-correlation energy was taken in the generalized gradient approximation (GGA) with the revised Perdew-Burke-Ernzerhof (PBEsol) functional [33]. A dense Monkhorst-Pack grid of k-special points was employed to perform integrations on the Brillouin zone (BZ) to obtain very well converged energies and forces. At selected volumes, the structures were fully relaxed to their optimized configuration through the calculation of the forces on atoms and the stress tensor. In the optimized configurations, the forces on the atoms were smaller than 0.006 eV $Å^{-1}$, and deviations of the stress tensor from a diagonal hydrostatic form were less than 0.1 GPa. Within the DFT formalism, the theoretical pressure, $P(V)$, can be determined at the same time as the total energy, $E(V)$, since P (like other derivatives of the energy) can be calculated from the stress. The obtained sets of volume, energy, and pressure data for each structure considered in this study were fitted with an equation of state. The electronic band structure along selected paths on the first BZ and the corresponding density of states (DOS) were calculated at different pressures.

Lattice-dynamics calculations were performed at the zone center (Γ point) of the BZ using the direct force constant approach. This method involves the construction of a dynamical matrix at the Γ point of the BZ. Separate calculations of the forces, with small displacements from the equilibrium configuration of the atoms within the primitive cell, are needed. The number of such independent displacements in the analyzed structures can be reduced by considering the crystal symmetry. Highly converged results on forces are required for the calculation of the dynamical matrix [34]. The subsequent diagonalization of the dynamical matrix provides the

frequencies of the normal modes. Moreover, these calculations allow identification of the symmetry and eigenvectors of the vibrational modes in each structure at the Γ point. To obtain the phonon dispersion curves, along high-symmetry directions of the BZ, and the phonon density of states (PDOS), we performed similar calculations using appropriate supercells, which allow the phonon dispersion at k-points to be obtained commensurate with the supercell size [34].

The elastic constants, C_{ij}, in the Voigt notation [35], were obtained by computing the macroscopic stress for a small strain with the use of the stress theorem [36]. For that purpose, the ground state and fully optimized structures at several pressures were strained in different directions according to their symmetry [37]. The total-energy variations were evaluated using a Taylor expansion for the total energy with respect to the applied strain [38]. Due to this fact, it is important to ensure that the strain used in the simulations guarantees the harmonic behavior. The generalized stability criteria were used in order to obtain information about the mechanical stability of the tetragonal phase of Bi_2O_3. The study of the generalized stability criteria applied to homogeneous crystals can provide important information on solid-solid structural transformations [39].

The topology of the electron density was calculated from the charge density obtained with VASP coupled to the CRITIC2 program [40], which enables both critical point location and basin integration. Relative errors in charge and volume integrations amount to a maximum of 10^{-6} and 10^{-4} arb. units, respectively. The number of critical points was in all cases coherent, providing a Morse sum equal to zero, as expected for a periodic system (see Table S1 in the Supplemental Material [41] for more details).

IV. RESULTS AND DISCUSSION

A. Optical absorption measurements

As already commented, a second-order IPT has been recently reported to occur in β-Bi_2O_3 near 2 GPa [26]. At the β-to-β' transition, the frequency of a zone-center soft optical mode goes to zero at the IPT pressure in a similar way to what happens in ferroelectric and ferroelastic phase transitions at different temperatures or pressures [42]. In ferroelectric phase transitions, usually a steep increase of the dielectric constant has been observed in the vicinity of the second-order phase transition because of the polar character of the soft mode [43]. On the other hand, no appreciable change of the dielectric constant has been observed in phase transitions where the soft mode has nonpolar character [42]. Figure 1 shows a selection of the experimental optical transmission curves of β-Bi_2O_3 at several pressures. As can be observed, no noticeable change of the maximum transmittance of the sample, which could be attributed to a notable change of the dielectric constant, occurs with increasing pressure as expected in a second-order IPT driven by a nonpolar soft mode [26]. Note that fluctuation of up to 5% in transmittance in measurements performed at different pressures is almost unavoidable due to the inaccuracy of the exact location of the light spot when the direct and transmitted intensity are measured at two different pressures. This fluctuation can be more important in compacted powders

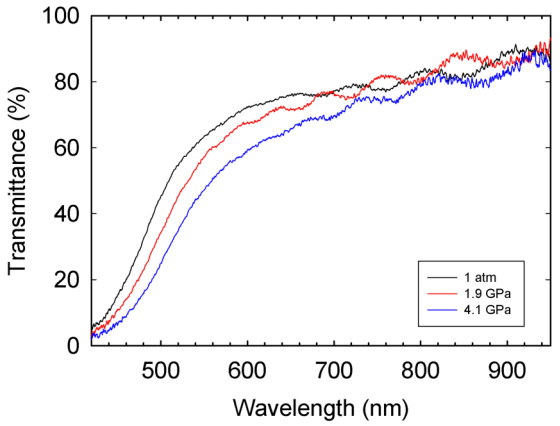

FIG. 1. Optical transmission spectra of β-Bi_2O_3 and β'-Bi_2O_3 at pressures below and above the IPT (around 2 GPa).

with irregular faces than in layered crystals, which can be perfectly exfoliated in samples with well-polished and parallel faces [44].

The optical absorption edge of β-Bi_2O_3 at room temperature and pressure has been measured in several works; however, there is no clear conclusion about the value of the indirect and direct bandgaps reported between 1.75 and 2.6 eV [45–47]. For this reason, we have calculated the electronic band structure and electronic DOS of β-Bi_2O_3 at room pressure [see Fig. 2(a)]. Calculated indirect and direct bandgaps (around 1.3 eV) are similar within 0.1 eV both without spin-orbit interaction and with spin-orbit interaction (not shown). Note that spin-orbit interaction is small for the case of Bi_2O_3 [48]. As can be observed, the conduction band (CB) shows considerable dispersion, and the conduction band minimum (CBM) is at the Γ point. In contrast, the top of the valence band (VB) is rather flat, and the valence band maximum (VBM) is between the M and Γ points of the BZ. The energy of the indirect bandgap is just 0.02 eV higher than the direct bandgap at the Γ point. The DOS reveals that the CBM has an important contribution of Bi $6p$ orbitals, followed by Bi $6s$ orbitals, whereas the VBM is dominated by O $2p$ orbitals, with some contribution of Bi $6s$ and $6p$ orbitals. Since allowed electric dipolar transitions correspond to transitions between bands where the change of orbital number $\Delta l = \pm 1$, our calculations show that both the direct and indirect bandgaps correspond to partially allowed transitions. On the other hand, the DOS of β'-Bi_2O_3 at 5 GPa [shown in Fig. 2(b)] is similar to that of β-Bi_2O_3 at room pressure, but with the VBM shifted from the Γ to the M point and with a larger energy difference between the VB maxima at the M and Γ points (0.32 eV). We want to stress that this energy difference increases up to 2 GPa and does not change appreciably above this pressure up to 27 GPa.

A selection of the optical absorption spectra in β-Bi_2O_3 under increasing pressure up to 26.7 GPa is shown in Fig. 3(a). As it can be observed, there is a red shift of the fundamental absorption edge with increasing pressure; however, there is a change in the slope of the high-absorption coefficient tail as pressure increases. This combination leads to a complex pressure dependence of the bandgap, as will be explained below. At this point, we just want to comment that our sample

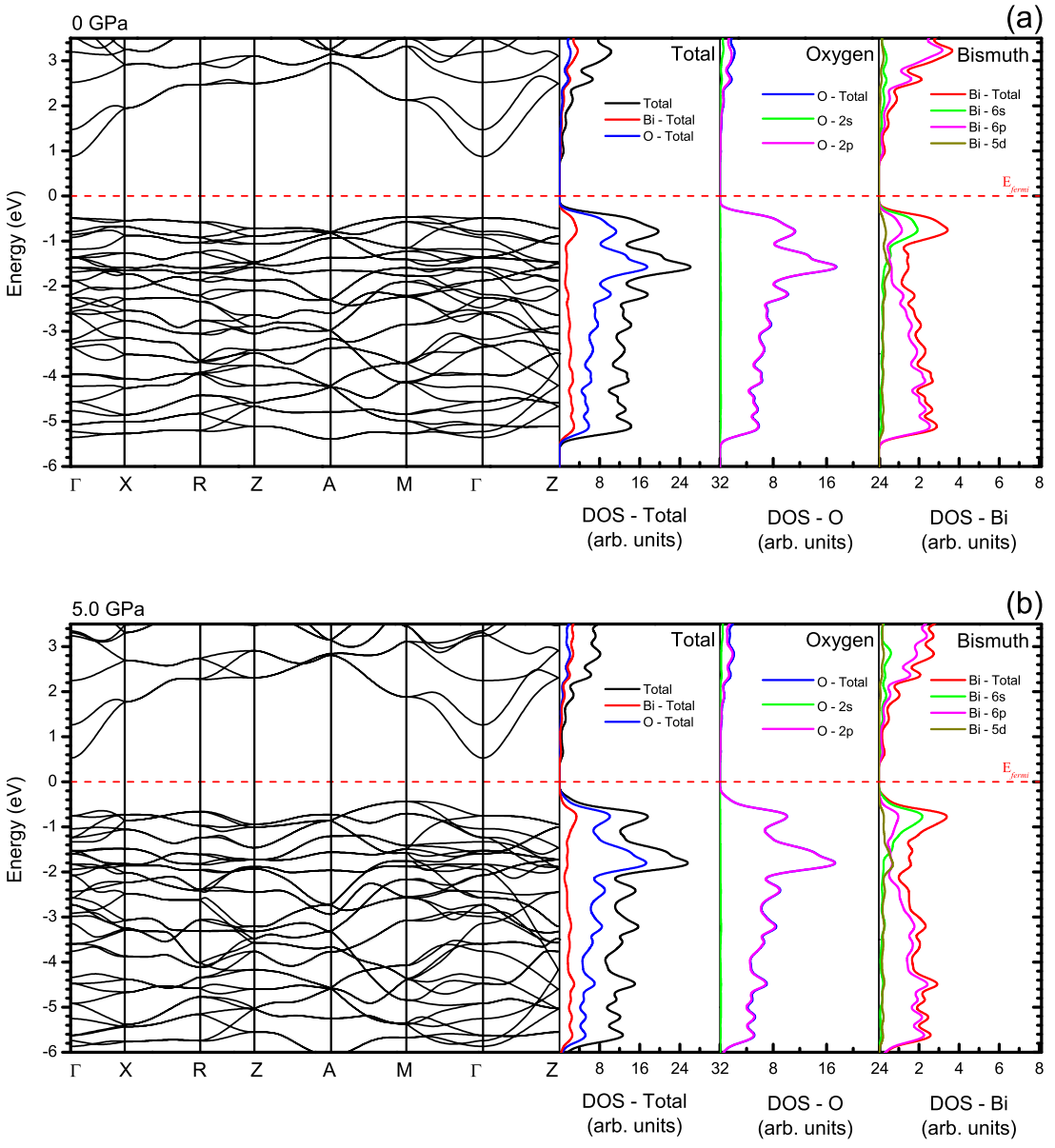

FIG. 2. Electronic band structure and density of states of β-Bi_2O_3 at 0 GPa (a) and of β'-Bi_2O_3 at 5.0 GPa (b).

is relatively thick (around 5 μm) to measure a direct bandgap. Therefore, we expect to see mainly evidence of the indirect bandgap in the fundamental absorption edge, which can be estimated by extrapolating a linear fit of $(\alpha \cdot h\nu)^{1/2}$ vs $h\nu$ to zero [see Fig. 3(b)]. It must be mentioned that despite the fact that this method does not give an accurate value of the bandgap energy, it yields a rather accurate value of the pressure coefficient of the bandgap energy [29].

Figure 4 shows the experimental pressure dependence of the indirect bandgap energy in β-Bi_2O_3 upon increasing (solid symbols) and decreasing (open symbols) pressure, as obtained from the extrapolation noted in the previous paragraph. Our estimated indirect bandgap is around 2.12(1) eV at room pressure, which is a value in between those given in the literature (between 1.75 and 2.6 eV) [45–47]. Note that *ab initio*–calculated bandgaps obtained within the DFT approximation are considerably underestimated, although the pressure dependence of the bandgap is well described [49]. For this reason, in order to compare the theoretical results with the experimental data, we shifted the theoretical curve of the indirect bandgap to match the experimental value of the indirect bandgap at room pressure (Fig. 4).

As observed in Fig. 4, there is a decrease of the experimental indirect bandgap up to 5–6 GPa and an increase above that pressure range. Both facts are in rather good agreement with the theoretical evolution of the indirect (solid line) bandgap. However, there is a notable deviation of the theoretical values of the indirect bandgap with respect to experimental values above 15 GPa. This is consistent with the phase transition observed above 15 GPa in a previous study [26]. Furthermore, the values of the extrapolated indirect bandgaps on decreasing pressure from 26.7 GPa (open symbols in Fig. 4) are larger than in original samples, thus indicating the nonreversibility of the compression process. This result gives support to the existence of a phase transition and its related PIA above 17–20 GPa as already reported [26]. Further support for the existence of

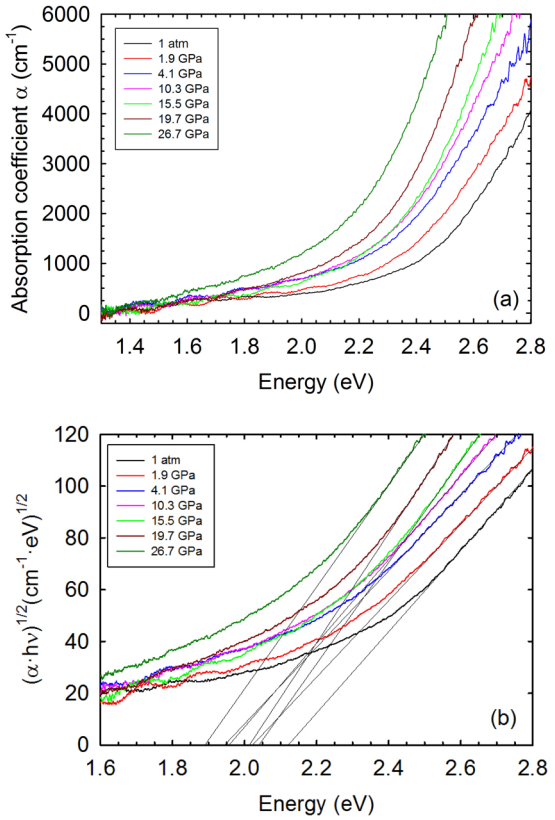

FIG. 3. (a) Optical absorption edge of β-Bi_2O_3 and β'-Bi_2O_3 on increasing pressure up to 26.7 GPa. (b) $(\alpha \cdot h\nu)^{1/2}$ vs $h\nu$ plot with extrapolated lines to determine the pressure dependence of the indirect M-Γ bandgap.

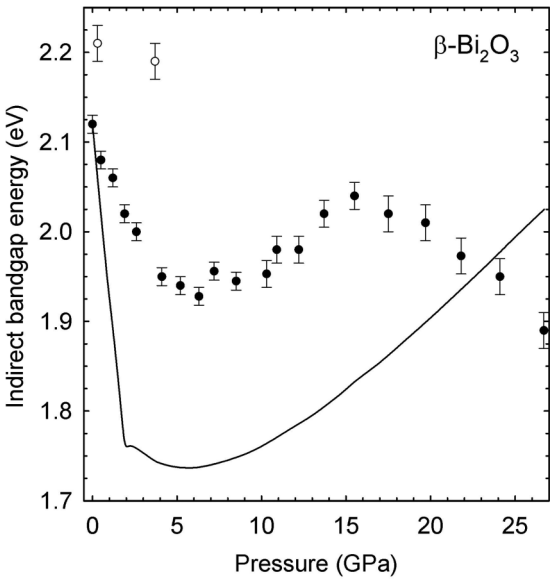

FIG. 4. Experimental (symbols) and theoretical (line) pressure dependence of the indirect M-Γ bandgap energy in β-Bi_2O_3 and β'-Bi_2O_3 both under increasing pressure (full symbols) and decreasing pressure (empty symbols). Theoretical calculations are upshifted to match the experimental indirect bandgap energy at room pressure.

this phase transition and PIA will be discussed in the next section.

B. Elastic properties

Compounds crystallizing in the structure of β-Bi_2O_3 (space group P-42_1c, No. 114) belong to the tetragonal Laue group TI. In this tetragonal symmetry, the stress-strain relations, given in the standard Voigt form, which describe the elastic behavior of the material, can be expressed as:

$$\begin{pmatrix}\sigma_{11}\\ \sigma_{22}\\ \sigma_{33}\\ \sigma_{23}\\ \sigma_{13}\\ \sigma_{12}\end{pmatrix} = \begin{pmatrix} C_{11} & C_{12} & C_{13} & & & \\ C_{12} & C_{11} & C_{13} & & & \\ C_{13} & C_{13} & C_{33} & & & \\ & & & C_{44} & & \\ & & & & C_{44} & \\ & & & & & C_{66}\end{pmatrix}\begin{pmatrix}e_{11}\\ e_{22}\\ e_{33}\\ e_{23}\\ e_{13}\\ e_{12}\end{pmatrix} \quad (1)$$

where σ_{ij} are usual stress components for $i,j = 1-3$ in Cartesian coordinates, and C_{ij} are the elastic constants. Displacements u_i are related to strain components e_{ij} by $e_{ii} = \partial u_i/\partial x_i$ and $e_{ij} = \partial u_i/\partial x_j + \partial u_j/\partial x_i$ when $i \neq j$. For a correct description of the elastic properties under homogeneous loading, like those at high hydrostatic pressures, elastic constants must be replaced by elastic stiffness coefficients B_{ij}, which can be readily obtained from elastic constants [50]. In the special case of hydrostatic pressure applied to a tetragonal crystal, the elastic stiffness coefficients are: $B_{11} = C_{11} - P$, $B_{12} = C_{12} + P$, $B_{13} = C_{13} + P$, $B_{33} = C_{33} - P$, $B_{44} = C_{44} - P$, and $B_{66} = C_{66} - P$, where P is the hydrostatic pressure. Note that the B_{ij} and C_{ij} coefficients are equal at 0 GPa. When the B_{ij} elastic stiffness coefficients are used, all the relations of the theory of elasticity can be applied for the crystal under any loading, including Born's stability conditions, which are identical in both loaded and unloaded states [50–55].

The theoretically calculated pressure dependence of the six elastic constants and elastic stiffness coefficients in β-Bi_2O_3 up to 1.9 GPa and in β'-Bi_2O_3 up to 26.7 GPa are shown in Figs. 5(a) and 5(b), respectively. Table I summarizes the set of six B_{ij} elastic stiffness coefficients as well as their linear and quadratic pressure coefficients in the β phase (at 0 GPa) and in the β' phase (at 2.3 GPa) as obtained from our *ab initio* calculations. Unfortunately, our theoretical values cannot be compared to experimental measurements in β-Bi_2O_3 even at room pressure; however, the set of elastic constants of glass Bi_2O_3 has been measured at 1 atm and 300 K, obtaining values of $C_{11} = 86.5$ GPa and $C_{44} = 26.5$ GPa [56]. Glass Bi_2O_3 has two independent elastic constants, C_{11} and C_{12}. Taking into account that $C_{44} = (C_{11} - C_{12})/2$, the C_{12} elastic constant of glass Bi_2O_3 is 33.5 GPa. These measurements show that experimental C_{11} and C_{12} values of glass Bi_2O_3 are 51% and 189% greater than C_{11} and C_{12} calculated for β-Bi_2O_3, respectively. On the other hand, experimental C_{44} of glass Bi_2O_3 is 18% smaller than C_{44} calculated for β-Bi_2O_3. We note that the discrepancies between the calculated elastic constants of β-Bi_2O_3 and those measured for glass Bi_2O_3 could be explained because the local environment of glass Bi_2O_3 is likely more similar to that of α-Bi_2O_3, the stable phase at room conditions, than to that of the metastable phase

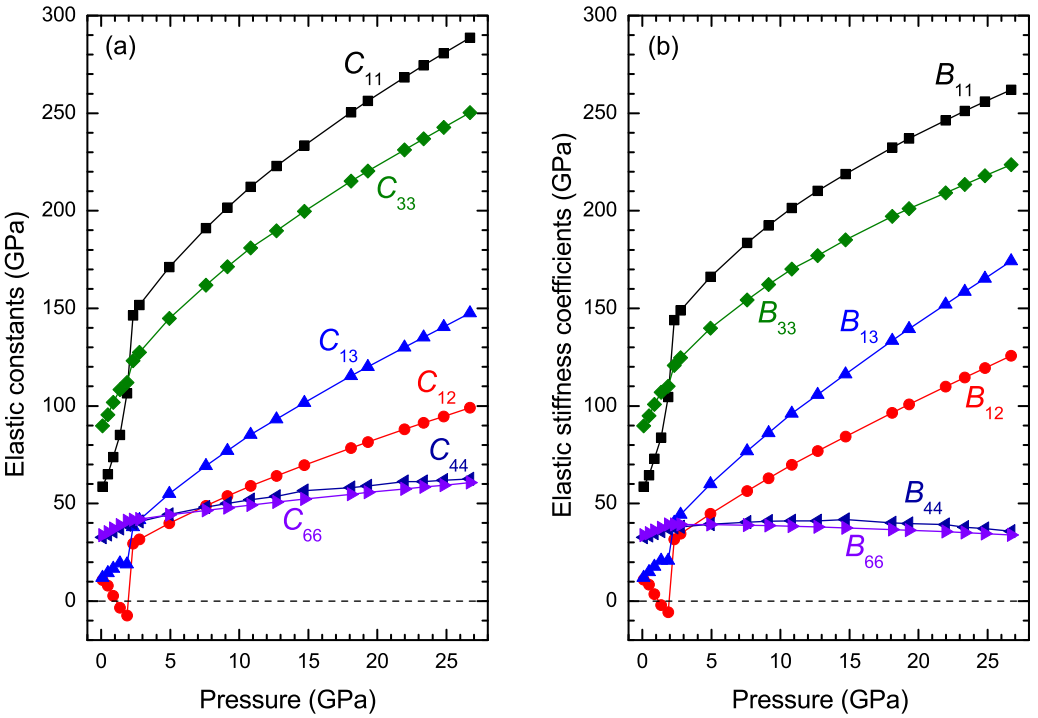

FIG. 5. Pressure dependence of the elastic constants (a) and elastic stiffness coefficients (b) in β-Bi_2O_3 and β'-Bi_2O_3. A clear change in the behavior of elastic constants and elastic stiffness coefficients is noted near 2 GPa, where the IPT between the two polymorphs is experimentally observed.

β-Bi_2O_3. A comparison of the theoretical elastic constants of monoclinic α-Bi_2O_3 with those of glass Bi_2O_3 is out of the scope of this work.

As observed in Fig. 5(b), all elastic stiffness coefficients show a positive linear pressure coefficient with increasing pressure in both β and β' phases, except B_{12} in the β phase, which shows a negative linear pressure coefficient and attains negative values for pressures above 1.1 GPa, and B_{66} in the β' phase, which shows a small negative linear pressure coefficient. The behavior of B_{12} will be discussed in the next section when we study the dynamic stability of β-Bi_2O_3. The most notable feature is that the pressure dependence of all elastic stiffness coefficients undergoes sudden and discontinuous changes near 2 GPa. This result can be interpreted as evidence of the β-to-β' IPT around this pressure, in good agreement with the present high-pressure optical absorption measurements and previous high-pressure XRD and RS measurements [26].

With the set of six elastic stiffness coefficients, standard formulas for the bulk (B) and shear (G) moduli for the tetragonal Laue group TI in the Voigt [57], Reuss [58], and Hill [59] approximations, labeled with subscripts V, R, and H, respectively, can be then applied [60]:

$$B_V = \frac{2B_{11} + B_{33} + 2B_{12} + 4B_{13}}{9} \tag{2}$$

$$B_R = \frac{1}{2S_{11} + S_{33} + 2S_{12} + 4S_{13}} \tag{3}$$

$$B_H = \frac{B_V + B_R}{2} \tag{4}$$

TABLE I. B_{ij} elastic stiffness coefficients and their linear and quadratic pressure coefficients a and b for the β phase (at 0 GPa) and the β' phase (at 2.3 GPa). Data were obtained by fitting the B_{ij} vs pressure data to the equation $B_{ij}(P) = B_{ij}(0) + a \cdot P + b \cdot P^2$ and $B_{ij}(P) = B_{ij}(2.3) + a \cdot (P - 2.3) + b \cdot (P - 2.3)^2$, respectively.

	β-Bi_2O_3			β'-Bi_2O_3		
	B_{ij} at 0 GPa (GPa)	a	b (GPa^{-1})	B_{ij} at 2.3 GPa (GPa)	a	b (GPa^{-1})
B_{11}	57.2(4)	14(1)	4.0(9)	144.7(4)	8.4(2)	−0.19(1)
B_{12}	11.6(6)	−6(2)	−3(1)	31.9(2)	4.95(6)	−0.060(5)
B_{13}	11.32(4)	7.5(1)	−0.48(8)	40.7(3)	7.4(1)	−0.109(8)
B_{33}	88.3(3)	14.6(9)	−0.7(6)	121.3(4)	7.1(2)	−0.16(1)
B_{44}	32.4(1)	2.6(3)		37.6(1)	0.77(2)	−0.043(2)
B_{66}	33.3(1)	3.3(4)		39.2(1)	−0.021(8)	−0.0098(6)

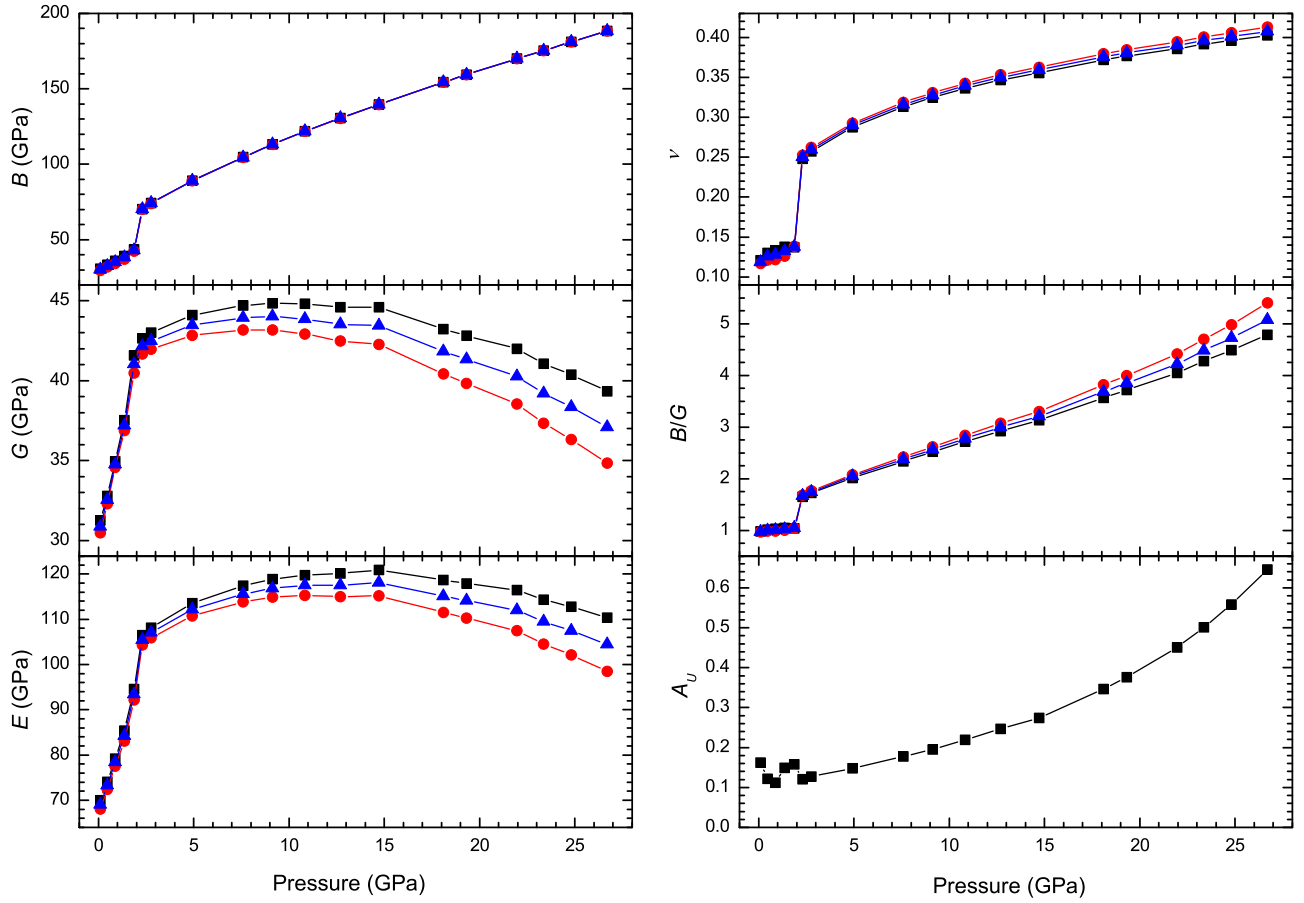

FIG. 6. Pressure dependence for the elastic moduli (B, G, E), Poisson's ratio (ν), and B/G ratio of β-Bi_2O_3 and β'-Bi_2O_3. Squares, circles, and triangles refer to the Voigt, Reuss, and Hill approximations, respectively. Data for the universal elastic anisotropy index (A_U) are plotted with squares.

$$G_V = \frac{2B_{11} + B_{33} - B_{12} - 2B_{13} + 6B_{44} + 3B_{66}}{15} \quad (5)$$

$$G_R = \frac{1}{8S_{11} + 4S_{33} - 4S_{12} - 8S_{13} + 6S_{44} + 3S_{66}} \quad (6)$$

$$G_H = \frac{G_V + G_R}{2} \quad (7)$$

For the case of the Reuss approximation, we use formulae where B_R and G_R are obtained from the components of the S_{ij} elastic compliances matrix, which is defined as the inverse of the B_{ij} matrix. In the Voigt and Reuss approximations, uniform strain or stress is assumed throughout the polycrystal, respectively [57,58]. Hill has shown that the Voigt and Reuss averages are limits and suggested that the actual effective B and G elastic moduli can be approximated by the arithmetic mean of the two bounds [59]. Young's (E) modulus and Poisson's ratio (ν) are calculated with the expressions [61,62]:

$$E_X = \frac{9B_X G_X}{G_X + 3B_X} \quad (8)$$

$$\nu_X = \frac{1}{2}\left(\frac{3B_X - 2G_X}{3B_X + G_X}\right) \quad (9)$$

where the subscript X refers to the symbols V, R, and H. Figure 6 shows the pressure dependence for the elastic moduli and Poisson's ratio of β-Bi_2O_3 and β'-Bi_2O_3. Table II contains the calculated values for the elastic moduli and Poisson's ratio of β-Bi_2O_3 at 0 GPa and of β'-Bi_2O_3 at 2.3 GPa in the Voigt, Reuss, and Hill approximations. It is interesting to note that the bulk modulus of β-Bi_2O_3 at 0 GPa in the Hill

TABLE II. Elastic moduli given in the Voigt, Reuss, and Hill approximations, labeled with subscripts V, R, and H, respectively, for β-Bi_2O_3 at 0 GPa and β'-Bi_2O_3 at 2.3 GPa. The Poisson's ratio (ν), B/G ratio, and universal elastic anisotropy index (A_U) are also given.

β-Bi_2O_3		β'-Bi_2O_3
	B_V, B_R, B_H (GPa)	
30.1, 29.1, 29.6		70.8, 70.6, 70.7
	G_V, G_R, G_H (GPa)	
30.9, 30.0, 30.4		42.7, 41.7, 42.2
	E_V, E_R, E_H (GPa)	
69.0, 67.0, 68.0		106.7, 104.5, 105.6
	ν_V, ν_R, ν_H	
0.12, 0.12, 0.12		0.25, 0.25, 0.25
	B_V/G_V, B_R/G_R, B_H/G_H	
0.98, 0.97, 0.97		1.66, 1.69, 1.68
	A_U	
0.18		0.12

approximation ($B_H = 29.6$ GPa) is in very good agreement with the value obtained from our *ab initio* structural data ($B_0 = 29.6$ GPa) and with the value obtained from high-pressure XRD measurements [$B_0 = 34(5)$ GPa] [26]. Therefore, these results give us confidence about the correctness of our elastic constant calculations in order to present further discussions.

From Fig. 6, it can be observed that there is a sudden increase of the Hill bulk modulus, B_H, from the β phase (43.0 GPa at 1.9 GPa) to the β' phase (70.7 GPa at 2.3 GPa), as expected for a second-order IPT. Similarly, there is a sudden increase of the Poisson's ratio, ν, from the β phase (0.14 at 1.9 GPa) to the β' phase (0.25 at 2.3 GPa). On the other hand, there is a continuous increase of the Hill shear modulus, G_H, from the β phase (30.4 GPa at 0 GPa) to the β' phase (42.2 GPa at 2.3 GPa). The same behavior is observed for the Hill Young's modulus, E_H, the value of which increases in a continuous way from the β phase (68.0 GPa at 0 GPa) to the β' phase (105.6 GPa at 2.3 GPa).

Figure 6 also shows the pressure dependence of the B/G ratio and the A_U universal elastic anisotropy index, defined as $A_U = 5G_V/G_R + B_V/B_R - 6$ [63] for both β-Bi_2O_3 and β'-Bi_2O_3. Table II summarizes the values of the B/G ratio and A_U for both β-Bi_2O_3 at 0 GPa and β'-Bi_2O_3 at 2.3 GPa. The ratio between the bulk and shear modulus, B/G, has been proposed by Pugh to predict brittle or ductile behavior of materials [64]. According to the Pugh criterion, a high B/G value indicates a tendency for ductility. If $B/G > 1.75$, then ductile behavior is predicted; otherwise, the material behaves in a brittle manner. In our particular case, we found a B/G ratio in the Hill approximation close to 1 in the β phase at 0 GPa and around 1.7 in the β' phase at 2.3 GPa (the value in the β' phase increases with increasing pressure). These values indicate that Bi_2O_3 is brittle in the β phase and ductile in the β' phase above 3.0 GPa.

The elastic anisotropy of crystals is of importance for both engineering science and crystal physics, since it is highly correlated to the possibility of inducing microcracks in the materials [65]. If A_U is equal to 0, no anisotropy exists. On the other hand, the more this parameter differs from 0, the more elastically anisotropic is the crystalline structure. Here, β-Bi_2O_3 at 0 GPa and β'-Bi_2O_3 at 2.3 GPa have A_U values slightly above 0; therefore, they are slightly anisotropic. As regards the pressure dependence of A_U, it is almost constant in the β phase and increases monotonically with increasing pressure in the β' phase; however, A_U only reaches 0.65 at 26.7 GPa, which indicates that β'-Bi_2O_3 has a rather small elastic anisotropy up to this pressure.

C. Mechanical and dynamical stability

We will first study the mechanical stability of β-Bi_2O_3 and β'-Bi_2O_3 at different pressures. At zero pressure, a lattice is mechanically stable only if the elastic energy change associated with an arbitrary deformation given by small strains is positive for any small deformation [66]. This implies restrictions on the C_{ij} elastic constants that are mathematically expressed by the fact that the principal minors of the determinant with elements C_{ij} are all positive. The latter restrictions are often called the Born-Huang stability criteria,

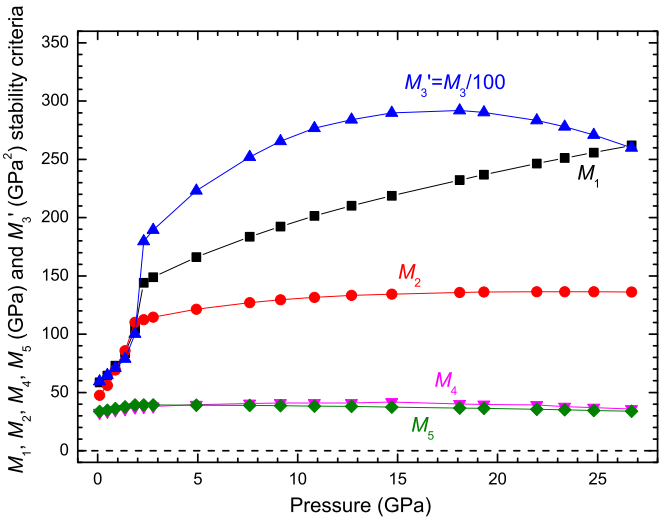

FIG. 7. Pressure dependence of the generalized stability criteria for β-Bi_2O_3 and β'-Bi_2O_3.

and, for the case of a tetragonal crystal with six C_{ij} elastic constants, mechanical stability requires that [66]:

$$C_{11} > 0, \quad C_{44} > 0, \quad C_{66} > 0, \quad C_{11} - C_{12} > 0 \tag{10}$$

and

$$C_{11}C_{33} + C_{12}C_{33} - 2{C_{13}}^2 > 0 \tag{11}$$

In our particular case, all the above criteria are satisfied, and β-Bi_2O_3 is mechanically stable at zero pressure as expected. In order to study the mechanical stability of this compound at high pressure, Eqs. (10) and (11) have to be modified to include the particular case when the external load is different from zero [50]. The five generalized stability criteria, M_i ($i = 1$ to 5), valid for a tetragonal crystal when the crystal is subjected to an external hydrostatic pressure P, take the form [50]:

$$M_1 = B_{11} > 0 \tag{12}$$

$$M_2 = B_{11} - B_{12} > 0 \tag{13}$$

$$M_3 = (B_{11} + B_{12})B_{33} - 2B_{13}^2 > 0 \tag{14}$$

$$M_4 = B_{44} > 0 \tag{15}$$

$$M_5 = B_{66} > 0 \tag{16}$$

with B_{ij} being the elastic stiffness coefficients. Figure 7 shows the evolution with pressure of the five generalized stability criteria in β-Bi_2O_3 and β'-Bi_2O_3. Generalized stability criteria are not violated either in β-Bi_2O_3 or in β'-Bi_2O_3 up to 26.7 GPa. Therefore, both tetragonal phases are mechanically stable under hydrostatic pressure up to 26.7 GPa.

Now we will study the dynamical stability of β-Bi_2O_3 and β'-Bi_2O_3 at high pressures. For this purpose, we present in Fig. 8 the phonon dispersion curves of β-Bi_2O_3 at 0, 1.4, and 1.9 GPa and curves of β'-Bi_2O_3 at 3.8, 15.7, and 26.7 GPa. It can be observed that at 0 GPa, there are several branches in β-Bi_2O_3 with imaginary frequencies near the Γ point.

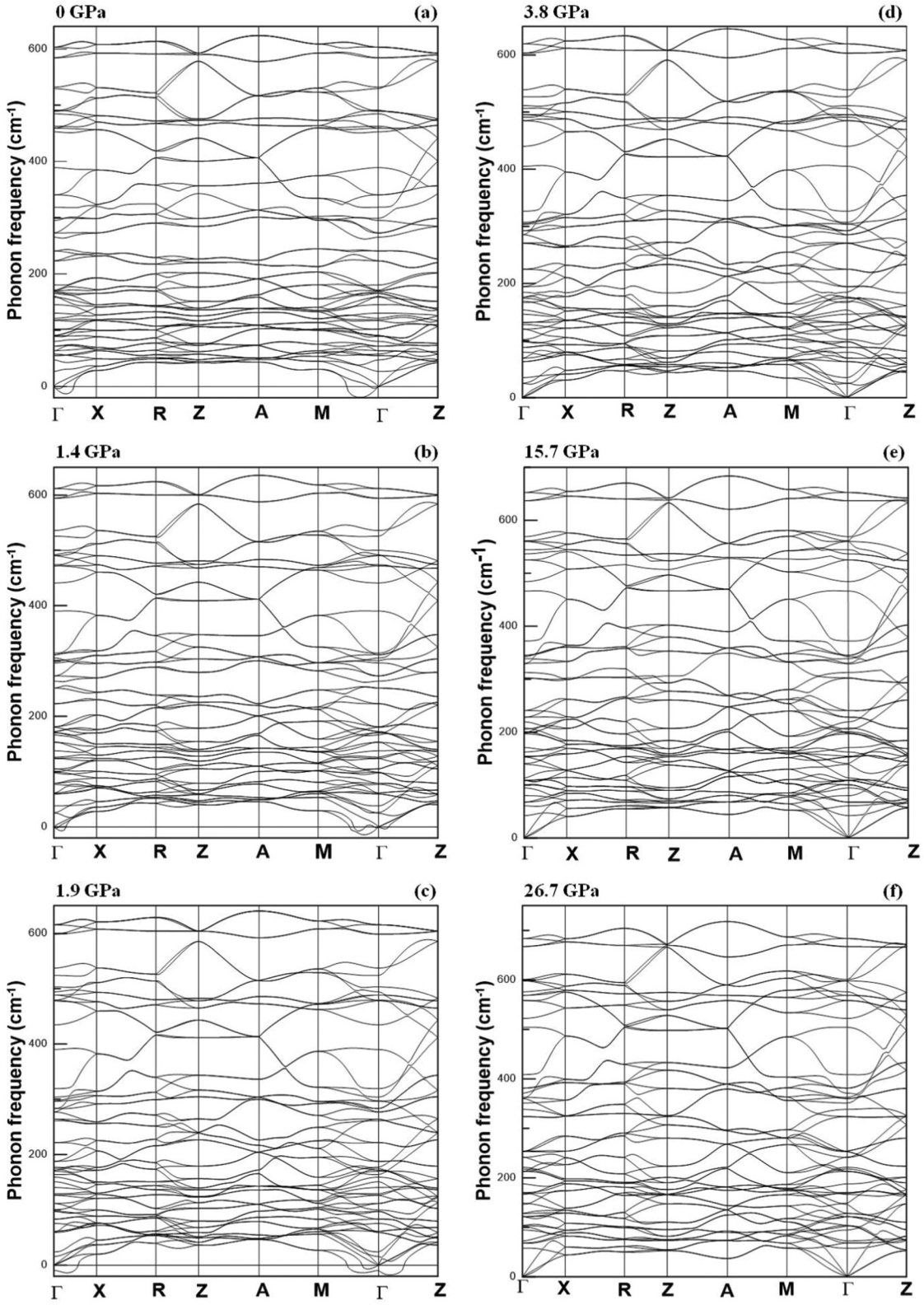

FIG. 8. Phonon dispersion curves of β-Bi_2O_3 at 0 GPa (a), 1.4 GPa (b), and 1.9 GPa (c), and of β'-Bi_2O_3 at 3.8 GPa (d), 15.7 GPa (e), and 26.7 GPa (f).

This result could be interpreted as a dynamical instability of β-Bi_2O_3. However, since β-Bi_2O_3 is a metastable phase at room conditions, we interpret the imaginary frequencies at 0 GPa to be a consequence of performing calculations in the quasiharmonic approximation at 0 K, which do not include the anharmonic interactions that are necessary for the stability of the lattice at finite temperatures. Note that similar theoretical imaginary frequencies were previously reported

for different Bi_2O_3 polymorphs by calculations at 0 GPa and 0 K [14].

Leaving aside the imaginary frequencies near Γ, our calculations at 1.4 and 1.9 GPa show an additional acoustic phonon branch along the Γ-Z direction that softens as pressure increases near Γ (long-wavelength modes) and reaches the maximum imaginary value around 1.9 GPa. The softening of this acoustic branch of β-Bi_2O_3 near Γ suggests that the second-order IPT near 2 GPa is in fact a ferroelastic phase transition between the low-symmetry β phase and the high-symmetry β' phase [42]. In this regard, a feature of the ferroelastic phase transition is that one of the acoustic branches near Γ goes to zero (not to imaginary frequencies), and, correspondingly, there is a decay of one elastic constant to zero [42]. Therefore, we ascribe the observation of the imaginary frequency of the soft acoustic branch and the observation of a negative value of the elastic stiffness coefficient B_{12} in the β phase to the lack of anharmonic contribution in our calculations. We consider that if anharmonic contributions would have been taken into account in our calculations, both the B_{12} elastic stiffness coefficient and the acoustic phonon frequency would approach the zero value at the IPT near 2 GPa.

On the other hand, calculations of phonon dispersion curves of β'-Bi_2O_3 at different pressures above 3.8 GPa show that all phonons have real frequencies that increase with increasing pressure at least up to 26.7 GPa. This means that β'-Bi_2O_3 is dynamically stable up to 26.7 GPa.

It is well known that the response of a material to compression could be sensitive to experimental conditions (e.g., deviatoric stresses, rate of compression, initial crystalline state, defects in the samples). As an example, it is known that the amorphization transition in α-SiO_2 is highly sensitive to the degree of nonhydrostaticity produced by the pressure-transmitting medium [67–70]. Therefore, it is advisable to perform experiments using powder and single crystals and with different pressure-transmitting media in order to fully understand the PIA process in a given material. In β-Bi_2O_3, we note that powder samples were used instead of single crystals because the β phase is a metastable phase that has been stabilized in submicron-sized particles and nanoparticles [71] and in N- and Y-doped Bi_2O_3 [22,72]. The use of gaseous environments (i.e., He or Ne) as pressure-transmitting media assures a larger hydrostatic regime than liquid media; however, some studies have shown that the use of gas can modify the compressibility of certain materials with porous or open framework structures when gas molecules can enter into the large voids of the crystalline structure with the increase of pressure, as in As_4O_6 [73], SiO_2 [74], and other porous materials [75]. In this regard, β-Bi_2O_3 contains large channels in its structure, which are formed by the presence of LEPs from Bi atoms. Therefore, these structural voids do not suggest the use of gaseous pressure-transmitting media with β-Bi_2O_3, since they could modify the structural properties under pressure. Consequently, we used in our experiments the more hydrostatic, nonpenetrating liquid pressure-transmitting medium available (methanol-ethanol-water mixture).

In order to help clarify the cause for PIA in β-Bi_2O_3, we carried out *ab initio* calculations. These calculations show that the β and β' phases are thermodynamically not competitive with respect to many other phases (see Fig. 9), including: the monoclinic α-Bi_2O_3-type structure [76] above 0 GPa; the trigonal HP-Bi_2O_3-type structure [77] above 0.5 GPa; the hexagonal HPC-Bi_2O_3-type structure [78] above 1.5 GPa; the trigonal A-type rare-earth sesquioxide (A-RES) structure [79] above 7.9 GPa; the orthorhombic Rh_2O_3-II-type structure [80] below 4.1 GPa and above 11.1 GPa; and the orthorhombic ε-Bi_2O_3-type structure [81] above 21.8 GPa (see Fig. 9). Since our calculations suggest that the β' structure is mechanically and dynamically stable under hydrostatic conditions, we can conclude that for our particular case of powder β'-Bi_2O_3 using methanol-ethanol-water as pressure-transmitting medium, the onset of PIA observed above 17–20 GPa in a previous work [26] must be likely related, on one hand, to the frustration of a reconstructive phase transition at room temperature and, on the other hand, to a mechanical or dynamical instability of this tetragonal phase against shear deformations occurring under nonhydrostatic conditions in powders. Observation of PIA in powders by nonhydrostatic stresses, which does not occur in single crystals, is well documented [82]. Further experiments at high pressure and high temperature could elucidate the nature of the high-pressure phase above 15 GPa, for which the transition from β'-Bi_2O_3 is frustrated at room temperature.

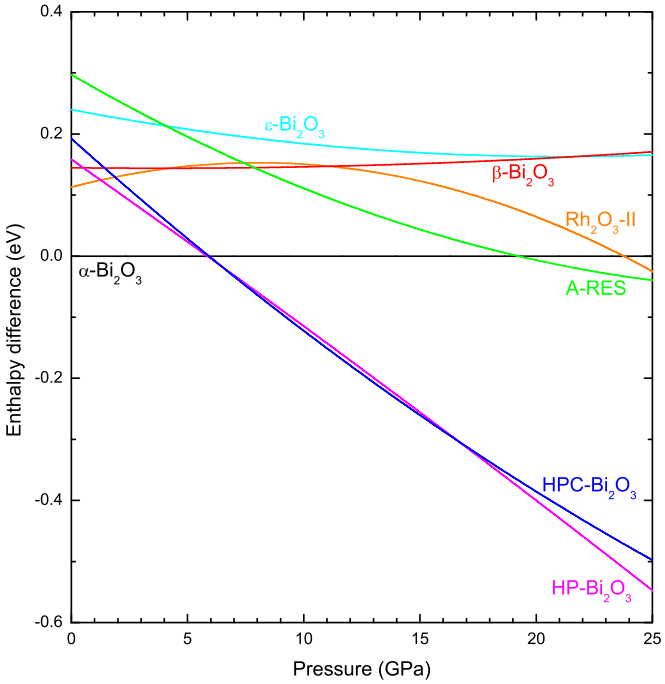

FIG. 9. Theoretical calculation of enthalpy difference vs pressure for different Bi_2O_3 phases. Enthalpy of monoclinic α-Bi_2O_3 is taken as the reference.

D. Chemical bond analysis

As a final study in this work, we performed an analysis of the topology of the theoretical electron density as obtained from our *ab initio* calculations in order to understand better the nature of the β-to-β' second-order IPT. It is well known that pressure-induced second-order phase transitions are characterized by a change in the compressibility, which can be

attributed to the microscopic behavior of atoms in the sample, and thus the electron density. A division of the system into atoms, with an associated atomic volume, can be done in terms of the electron density, following what is known as the atoms in molecules (AIM) approach [83].

In an ordinary molecule, the electron density has maxima (cusps) at the nuclei and decays exponentially as the electron density moves away from the nuclei. The resulting topology of the molecular density looks like an assemblage of mountains, each of which is identified as an atom. Within this approach, one identifies chemical bonds with the valleys (bond paths) in between mountains. The lowest point in the valley (first-order saddle point) is also known as the bond critical point (BCP). Using this approach, atoms are well defined in three dimensions, and it is possible to integrate the properties of each atom and obtain their corresponding atomic volume and charge.

It has been proposed that IPTs are related to changes in the bonding pattern (in the number of BCPs) without changes either in the space group or in the Wyckoff positions [84]. Most commonly, critical points come close together upon compression and collapse at the IPT (also known as cusp catastrophe), yielding a different number of critical points and a different compressibility behavior before and after the transition pressure. However, analysis of the topology of the electron density in β-Bi_2O_3 demonstrates that this condition is not necessary, since the number of critical points is maintained along the β-to-β' IPT despite their symmetry changes (see Table S1 in the Supplemental Material [41]). More specifically, there is a rise in the point symmetry of the critical points in the β' phase with respect to the β phase. An equalization of Bi-O1 distances is observed (see Fig. S1 in the Supplemental Material [41]): The first and second O1 neighbors around Bi atoms are different in phase β and become equal in phase β'. Moreover, in spite of Bi-O1 and Bi-O2 distances being different, the electron density at their corresponding BCPs becomes very similar, with no associated cusp catastrophe (see Fig. S2 in the Supplemental Material [41]), unlike what was previously assumed [85].

Since we are looking at a change in compressibility, and Bader atomic volumes are well defined, it is possible to track the IPT in terms of Bader atomic compressibility changes. Figure S3(a) in the Supplemental Material [41] shows the evolution of the atomic volumes in β-Bi_2O_3 under pressure. As observed, the absolute changes at the IPT near 2 GPa are small, so we have plotted in Fig. 10(a) the pressure dependence of the atomic volumes where the atomic volume at zero pressure has been subtracted for comparison purposes. As can be seen, there is a change in the atomic compressibilities that accompanies the β-to-β' transition. In addition, in the β phase, the atomic volume of O1 decreases at a larger rate than that of O2; however, in the β' phase, both atomic volumes decrease at a similar rate because the electron density at the BCP along the different Bi-O bonds becomes similar (see Fig. S2 in the Supplemental Material [41]) in spite of O1 and O2 having slightly different atomic volumes and charges {see Fig. S3(a) and S3(b), respectively, in the Supplemental Material [41]}.

The change in the electronic structure at the IPT can also be followed by inspection of the atomic charges {see Fig. S3(b) in the Supplemental Material [41]}. Again, due to the small absolute changes in atomic charges, it is more convenient to plot the relative changes of the atomic charges with respect to the value of zero pressure [see Fig. 10(b)]. It can be observed that whereas charges of atoms O1 and O2 exhibit a very different behavior in the β phase, they follow almost the same pattern in the β' phase in spite of their slightly different absolute values.

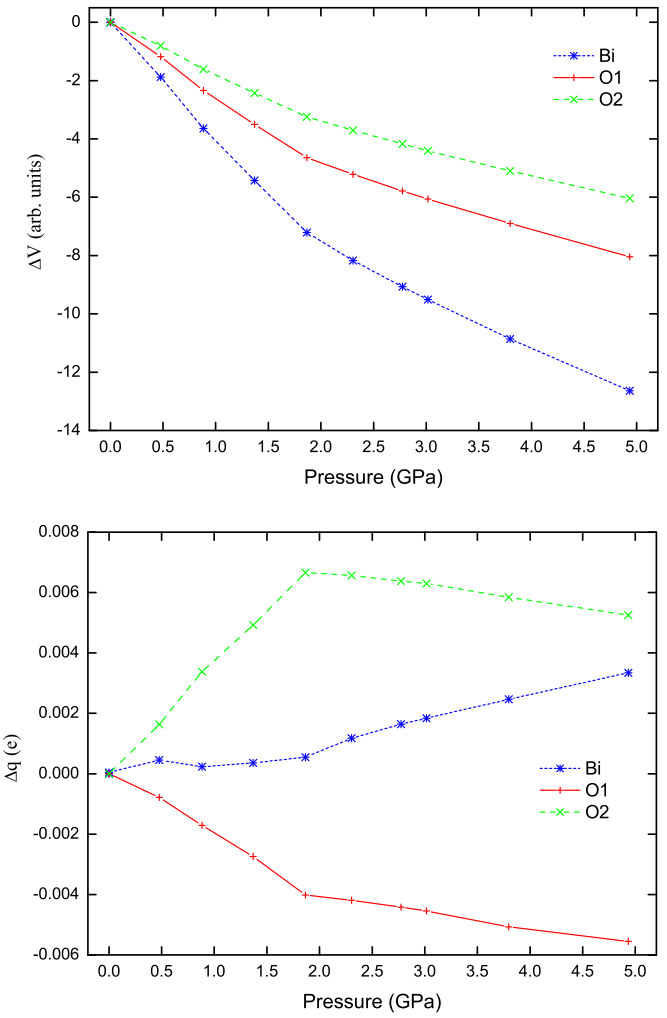

FIG. 10. Evolution of Bader relative volumes (a) and relative charges (b) with respect to zero pressure in the atomic basins of β-Bi_2O_3 upon compression. O1 and O2 labels represent oxygen atoms located at the Wyckoff positions 8*e* and 4*d*, respectively.

In summary, the results of the topological analysis of the electron density highlight that (i) the response of the O1 and O2 atoms to pressure is rather different in the β phase and becomes very similar in the β' phase, in good agreement with the increase of structural symmetry observed in the pressure-induced β-to-β' transition, and (ii) the IPT is driven by an equalization of the electron densities at the BCPs of the different Bi-O bonds and not by the existence of a cusp catastrophe.

V. CONCLUSIONS

We have performed an experimental and theoretical study of the optical properties of tetragonal bismuth oxide (β-Bi_2O_3) at high pressure by means of optical transmission measurements

combined with *ab initio* electronic band structure calculations. We have measured and calculated the pressure dependence of the indirect bandgap of β-Bi_2O_3. The obtained results are consistent with previous reports of the second-order β-to-β' IPT in Bi_2O_3 near 2 GPa and with the phase transition and possible PIA around 15 and 17–20 GPa, respectively [26]. We have also theoretically studied the pressure dependence of the elastic stiffness coefficients of β-Bi_2O_3 and β'-Bi_2O_3. An abrupt change of elastic stiffness coefficients is found near 2 GPa, which gives additional support to the IPT already noted. The mechanical and dynamical stability of the tetragonal structure of β-Bi_2O_3 and β'-Bi_2O_3 has been theoretically studied at high pressure. Both phases are found to be mechanically stable under hydrostatic conditions in the studied pressure range. However, β-Bi_2O_3 is dynamically unstable near 2 GPa. The dynamical instability leads to a ferroelastic (β-to-β') phase transition, in good agreement with the experimentally observed features of the IPT. On the other hand, β'-Bi_2O_3 is dynamically stable at least up to 26.7 GPa under hydrostatic conditions; thus, the possible PIA observed above 17–20 GPa in powder β'-Bi_2O_3 using methanol-ethanol-water as pressure-transmitting medium is likely related, on one hand, to the frustration of a reconstructive phase transition at room temperature and, on the other hand, to a mechanical or dynamical instability of this tetragonal phase against shear deformations occurring under nonhydrostatic conditions in powders. Finally, our study of the topology of the theoretical electron density shows that the ferroelastic IPT is not caused by a cusp catastrophe, but by the equalization of the electron densities of both independent O atoms in the unit cell at the bond critical points along the different Bi-O bonds.

ACKNOWLEDGMENTS

This work was performed with financial support from the Spanish Ministerio de Economía y Competitividad under Projects No. MAT2013-46649-C4-2/3-P and No. MAT2015-71070-REDC. This publication is the fruit of "Programa de Valoración y Recursos Conjuntos de I+D+i VLC/CAMPUS" and was financed by the Spanish Ministerio de Educación, Cultura y Deporte as part of "Programa Campus de Excelencia Internacional" through Projects No. SP20140701 and No. SP20140871 and by the Brazilian Conselho Nacional de Desenvolvimento Científico e Tecnológico (CNPq) under Project No. 201050/2012-9. Supercomputer time was provided by the Red Española de Supercomputación (RES) and the MALTA cluster. J.A.S. acknowledges financial support through the Juan de la Cierva fellowship (JCI-2011-09781).

[1] Z. Ai, Y. Huang, S. Lee, and L. Zhang, J. Alloys Compd. **509**, 2044 (2011).
[2] Y. Bessekhouad, D. Robert, and J. V. Weber, Catal. Today **101**, 315 (2005).
[3] A. Cabot, A. Marsal, J. Arbiol, and J. R. Morante, Sensors Actuators B **99**, 74 (2004).
[4] L. Zhou, W. Z. Wang, H. L. Xu, S. M. Sun, and M. Shang, Chem. Eur. J. **15**, 1776 (2009).
[5] F. L. Zheng, G. R. Li, Y. N. Ou, Z. L. Wang, C. Y. Su, and Y. X. Tong, Chem. Commun. **46**, 5021 (2010).
[6] Y. D. Liu, F. Xin, F. M. Wang, S. X. Luo, and X. H. Yin, J. Alloys Compd. **498**, 179 (2010).
[7] S. S. Bhande, R. S. Mane, A. V. Ghule, and S. H. Han, Scripta Mat. **65**, 1081 (2011).
[8] A. Orera, and P. R. Slater, Chem. Mat. **22**, 675 (2010).
[9] P. Shuk, H. D. Wiemhofer, U. Guth, W. Gopel, and M. Greenblatt, Solid State Ionics **89**, 179 (1996) and references therein.
[10] S. Hull, Rep. Prog. Phys. **67**, 1233 (2004).
[11] N. Chanthima, J. Kaewkhao, C. Kedkaew, W. Chewpraditkul, A. Pokaipist, and P. Limsuwan, Prog. Nucl. Sci. Technol. **1**, 106 (2011).
[12] K. Won-in, S. Pongkrapan, and P. Dararutana, Mat. Sci. Forum **695**, 223 (2011).
[13] T. Maeder, Int. Mat. Rev. **58**, 3 (2013).
[14] A. Matsumoto, Y. Koyama, and I. Tanaka, Phys. Rev. B: Condens. Matter Mater. Phys. **81**, 094117 (2010).
[15] A. Matsumoto, Y. Koyama, A. Togo, M. Choi, and I. Tanaka, Phys. Rev. B: Condens. Matter Mater. Phys. **83**, 214110 (2011).
[16] G. Catalan and J. F. Scott, Adv. Mater. **21**, 2463 (2009).
[17] S. Iyyapushpam, S. T. Nishanthi, and D. P. Padiyan, Mat. Lett. **86**, 25 (2012).
[18] L. Cheng and Y. Kang, J. Alloys Compd. **585**, 85 (2014).
[19] Y. Yan, Z. Zhou, Y. Cheng, L. Qiu, C. Gao, and J. Zhou, J. Alloys Compd. **605**, 102 (2014).
[20] H. Cheng, B. Huang, J. Lu, Z. Wang, B. Xu, X. Qin, X. Zhang, and Y. Dai, Phys. Chem. Chem. Phys. **12**, 15468 (2010).
[21] K. Brezesinski, R. Ostermann, P. Hartmann, J. Perlich, and T. Brezesinski, Nanofiber Mats. Chem. Mater. **22**, 3079 (2010).
[22] X. Liu, H. Deng, W. Yao, Q. Jiang, and J. Shen, J. Alloy. Comp. **651**, 135 (2015).
[23] T. T. Li, and S. L. Luo, Ceram. Inter. **41**, 13135 (2015).
[24] M. Li, F. Li, and P. G. Yin, Chem. Phys. Lett. **601**, 92 (2014).
[25] Z. Zhao, Q. Zeng, H. J. Zhang, S. B. Wang, S. Hirai, Z. D. Zeng, and W. L Mao, Phys. Rev. B **91**, 184112 (2015).
[26] A. L. J. Pereira, J. A. Sans, R. Vilaplana, O. Gomis, F. J. Manjón, P. Rodríguez-Hernández, A. Muñoz, C. Popescu, and A. Beltrán, J. Phys. Chem. C **118**, 23189 (2014).
[27] R. Letoullec, J. P. Pinceaux, and P. Loubeyre, High Press. Res. **1**, 77 (1988).
[28] M. K. Mao, J. Xu, and P. M. Bell, J. Geophys. Res. **91**, 4673 (1986).
[29] O. Gomis, R. Vilaplana, F. J. Manjón, J. Ruiz-Fuertes, E. Pérez-González, J. López-Solano, E. Bandiello, D. Errandonea, A. Segura, P. Rodríguez-Hernández, A. Muñoz, V. V. Ursaki, and I. M. Tiginyanu, Phys. Status Solidi B **252**, 2043 (2015).
[30] P. Hohenberg and W. Kohn, Phys. Rev. **136**, B864 (1964).
[31] G. Kresse and J. Hafner, Phys. Rev. B **47**, 558 (1993).
[32] P. E. Blöchl, Phys. Rev. B **50**, 17953 (1994).
[33] J. P. Perdew, A. Ruzsinszky, G. I. Csonka, O. A. Vydrov, G. E. Scuseria, L. A. Constantin, X. Zhou, and K. Burke, Phys. Rev. Lett. **100**, 136406 (2008).
[34] K. Parlinski, Z.-Q. Li, and Y. Kawazoe, Phys. Rev. Lett. **78**, 4063 (1997).

[35] J. F. Nye, *Physical Properties of Crystals: Their Representation by Tensor and Matrices* (Oxford University Press, Oxford, UK, 1957).

[36] N. Chetty, A. Muñoz, and R. M. Martin, Phys. Rev. B **40**, 11934 (1989).

[37] Y. Le Page and P. Saxe, Phys. Rev. B **65**, 104104 (2002).

[38] O. Beckstein, J. E. Klepeis, G. L. W. Hart, and O. Pankratov, Phys. Rev. B **63**, 134112 (2001).

[39] M. A. Carpenter and E. K. H. Salje, Eur. J. Mineral **10**, 693 (1998).

[40] A. Otero-de-la-Roza, E. R. Johnson, and J. Contreras-García, Phys. Chem. Chem. Phys. **14**, 12165 (2012).

[41] See Supplemental Material at http://link.aps.org/supplemental/10.1103/PhysRevB.93.224111 for results from the chemical bond analysis. It contains the evolution of distance (Fig. S1), electron density at the BCP (Fig. S2), volume (Fig. S3a), and charge (Fig. S3b) upon compression. A list of critical points is given in Table S1.

[42] G. A. Samara and P. S. Peercy, The Study of Soft-Mode Transitions at High Pressure, *Solid State Physics* (Academic Press, New York, 1982), Vol. 36, pp. 1–118.

[43] G. A. Samara, Phys. Rev. B **1**, 3777 (1970).

[44] F. J. Manjón, D. Errandonea, A. Segura, V. Muñoz, G. Tobias, P. Ordejón, and E. Canadell, Phys. Rev. B **63**, 125330 (2001).

[45] V. Dolocan, Appl. Phys. **16**, 405 (1978).

[46] V. Dolocan and F. Iova, Phys. Status Solidi A **64**, 755 (1981).

[47] J. George, B. Pradeep, and K. S. Joseph, Phys. Status Solidi A **103**, 607 (1987).

[48] A. L. J. Pereira, O. Gomis, J. A. Sans, J. Pellicer-Porres, F. J. Manjón, A. Beltrán, P. Rodríguez-Hernández, and A. Muñoz, J. Phys.: Condens. Matter **26**, 225401 (2014).

[49] X. Zheng, A. J. Cohen, P. Mori-Sánchez, X. Q. Hu, and W. T. Yang, Phys. Rev. Lett. **107**, 026403 (2011).

[50] G. Grimvall, B. Magyari-Köpe, V. Ozoliņš, and K. A. Persson, Rev. Mod. Phys. **84**, 945 (2012).

[51] J. Wang, S. Yip, S. R. Phillpot, and D. Wolf, Phys. Rev. Lett. **71**, 4182 (1993).

[52] J. Wang, J. Li, S. Yip, S. Phillpot, and D. Wolf, Phys. Rev. B **52**, 12627 (1995).

[53] Z. Zhou and B. Joós, Phys. Rev. B **54**, 3841 (1996).

[54] B. B. Karki, L. Stixrude, and R. M. Wentzcovitch, Rev. Geophys. **39**, 507 (2001).

[55] O. M. Krasil'nikov, M. P. Belov, A. V. Lugovskoy, I. Yu. Mosyagin, and Yu. Kh. Vekilov, Comput. Mat. Sci. **81**, 313 (2014).

[56] J. Philip, N. Rodrigues, M. Sadhukan, A. K. Bera, and B. K. Chaudhuri, J. Mat. Sci. **35**, 229 (2000).

[57] W. Voigt, *Lehrbuch der Kristallphysik* (Teubner, Leipzig, 1928).

[58] A. Reuss and Z. Angew, Math. Mech. **9**, 49 (1929).

[59] R. Hill, Phys. Soc. London A **65**, 349 (1952).

[60] R. Caracas and T. B. Ballaran, Phys. Earth Planet. Inter. **181**, 21 (2010).

[61] Q. J. Liu, Z. T. Liu, and L. P. Feng, Commun. Theor. Phys. **56**, 779 (2011).

[62] O. Gomis, D. Santamaría-Pérez, J. Ruiz-Fuertes, J. A. Sans, R. Vilaplana, H. M. Ortiz, B. García-Domene, F. J. Manjón, D. Errandonea, P. Rodríguez-Hernández, A. Muñoz, and M. Mollar, J. Appl. Phys. **116**, 133521 (2014).

[63] S. I. Ranganathan and M. Ostoja-Starzewski, Phys. Rev. Lett. **101**, 055504 (2008).

[64] S. F. Pugh, Philos. Mag. **45**, 823 (1954).

[65] V. Tvergaard and J. W. Hutchinson, J. Am. Ceram. Soc. **71**, 157 (1988).

[66] M. Born, Proc. Cambridge Philos. Soc. **36**, 160 (1940).

[67] K. J. Kingma, R. J. Hemley, H.-k. Mao, and D. R. Veblen, Phys. Rev. Lett. **70**, 3927 (1993).

[68] L. Huang, M. Durandurdu, and J. Kieffer, Nat. Mater. **5**, 977 (2006).

[69] D. Machon, F. Meersman, M. C. Wilding, M. Wilson, and P. F. McMillan, Prog. Mater. Sci. **61**, 216 (2014).

[70] J. Wang, Z. Mao, F. Jiang, and T. S. Duffy, Phys. Chem. Miner. **42**, 203 (2015).

[71] X. Xiao, R. Hu, S. Tu, C. Zheng, H. Zhong, X. Zuo, and J. Nan, RSC Adv. **5**, 38373 (2015).

[72] Y. G. Lu, Y. C. Yang, Z. X. Ye, and S. Y. Liu, J. Inorg. Mater. **27**, 643 (2012).

[73] J. A. Sans, F. J. Manjón, C. Popescu, V. P. Cuenca-Gotor, O. Gomis, A. Muñoz, P. Rodríguez-Hernández, J. Contreras-García, J. Pellicer-Porres, A. L. J. Pereira, D. Santamaría-Pérez, and A. Segura, Phys. Rev. B **93**, 054102 (2016).

[74] T. Sato, N. Funamori, and T. Yagi, Nat. Comm. **2**, 345 (2011).

[75] H. Furukawa, N. Ko, Y. Bok Go, N. Aratani, S. Beom Choi, E. Choi, A. Ö. Yazaydin, R. Q. Snurr, M. O'Keeffe, J. Kim, and O. M. Yaghi, Science **329**, 424 (2010).

[76] A. L. J. Pereira, D. Errandonea, A. Beltrán, L. Gracia, O. Gomis, J. A. Sans, B. García-Domene, A. Miquel-Veyrat, F. J. Manjón, A. Muñoz, and C Popescu, J. Phys.: Condens. Matter **25**, 475402 (2013).

[77] S. Ghedia, T. Locherer, R. Dinnebier, D. L. V. K. Prasad, U. Wedig, M. Jansen, and A. Senyshyn, Phys. Rev. B **82**, 024106 (2010).

[78] T. Locherer, D. L. V. K. Prasad, R. Dinnebier, U. Wedig, M. Jansen, G. Garbarino, and T. Hansen, Phys. Rev. B **83**, 214102 (2011).

[79] T. Atou, H. Faqir, M. Kikuchi, H. Chiba, and Y. Syono, Mater. Res. Bull. **33**, 289 (1998).

[80] B. García-Domene, J. A. Sans, O. Gomis, F. J. Manjón, H. M. Ortiz, D. Errandonea, D. Santamaría-Pérez, D. Martínez-García, R. Vilaplana, A. L. J. Pereira, A. Morales-García, P. Rodríguez-Hernández, A. Muñoz, C. Popescu, and A. Segura, J. Phys. Chem. C **118**, 20545 (2014).

[81] N. Cornei, N. Tancret, F. Abraham, and O. Mentre, Inorg. Chem. **45**, 4886 (2006).

[82] S. Ekbundit, K. Leinenweber, J. L. Yarger, J. S. Robinson, M. Verhelst-Voorhees, and G. H. Wolf, J. Solid State Chem. **126**, 300 (1996).

[83] R. F. W. Bader, *Atoms in Molecules. A Quantum Theory* (Clarendon Press, Oxford, UK, 1990).

[84] T. E. Jones, M. E. Eberhart, and D. P. Clougherty, Phys. Rev. Lett. **105**, 265702 (2010).

[85] V. Dmitriev, in *High-Pressure Crystallography: From Fundamental Phenomena to Technological Applications*, edited by E. Boldyreva and P. Dera (Springer, Berlin, 2010), p. 171.